Influence of defects on the valley polarization properties of monolayer MoS₂ grown by chemical vapor deposition

Faiha Mujeeb , Poulab Chakrabarti, Vikram Mahamiya , Alok Shukla, and Subhabrata Dhar[*]
Department of Physics, Indian Institute of Technology Bombay, Mumbai 400076, India

Temperature-dependent polarization-resolved photoluminescence spectroscopy is carried out on as-grown, transferred, and coated 1L-MoS₂ samples grown by the chemical vapor deposition technique to explore the underlying mechanism behind the valley depolarization process. It has been found that the momentum scattering of the excitons due to the sulfur-vacancies-attached-with-air-molecules type of defects has a strong influence in the suppression of valley polarization. Our study reveals that at sufficiently low densities of such defects and temperatures, the long-range electron-hole exchange mediated intervalley transfer of excitons via the Maialle-Silva-Sham (MSS) mechanism, as suggested by a recent theory [Yu and Wu, Phys. Rev. B **89**, 205303 (2014)], is indeed the most dominant spin-flip process. In the process, the momentum scattering of the excitons by the defects takes the central stage. Interestingly, the study finds the scattering rate to be proportional to the cube root of the density of the defects. The intervalley transfer process of excitons involving the Γ valley also has significance in valley depolarization, especially when the layer is either under a tensile strain or has a high density of V_S defects, as these perturbations reduces K to Γ-energy separation. Band-structural calculations carried out within a density functional theory framework validate these findings. The study further suggests that exchange interactions with the physisorbed oxygen molecules can result in the intervalley spin-flip scattering of the excitons and this process gives an important contribution to valley depolarization, especially at the strong scattering regime.

I. INTRODUCTION

Two-dimensional transition-metal dichalcogenides (TMDs) offer a valley degree of freedom, which can be exploited to design next-generation valley-based electronics or "valleytronics" [1]. The broken inversion symmetry, together with strong spin-orbit coupling, results in the valley-dependent optical selection rules in monolayer (1L)-MoS₂. This property enables an exciton to sustain its valley character throughout the time of its existence. In fact, valley polarization approaching 100% has been reported in exfoliated 1L-MoS₂ samples [1–5], whereas 1L-MoS₂ films grown by the chemical vapor deposition (CVD) technique, which is frequently used to grow large area films on different substrates, show only moderate polarization values (less than 50%) [6]. Since large area coverage of the monolayer film has to be ensured for any practical application of the material, it is imperative to understand the reason for the moderation of valley polarization in CVD-grown 1L-MoS₂. Note that the optical and electrical properties of CVD-grown layers often suffer from the presence of a high density of sulfur vacancy defects (V_S) and the residual strain [7–13]. Since the valley and spin properties are closely related to the crystal symmetry, both the strain [13,14] and the defects [15–18] are expected to have certain impacts on the valley polarization (VP) property of 1L-MoS₂ grown by the CVD technique. It has

indeed been experimentally demonstrated that VP decreases with increasing tensile strain in the 1L-MoS₂ [13,14]. This has been explained in terms of longitudinal acoustic (LA) phonon-assisted intervalley scattering of the excitons via the Γ valley as the K to Γ-valley energy separation decreases with the increase of biaxial tensile strain [19,20]. However, the underlying mechanism through which defects govern VP in this system is yet to be systematically investigated.

There have been several theoretical studies to understand the valley depolarization process in transition-metal dichalcogenides [21–23]. Recently, theoretical focus has been on the satellite valley effects [24] and phonon-limited valley polarization [25]. In an ideal scenario, bright excitons generated in one of the K valleys through circularly polarized (σ^+ or σ^- polarization) photons, are expected to stay in the same valley until recombination. One may think that intervalley phonon scattering along with spin flipping of both the electron and hole are necessary to transfer a bright exciton between K to K' valleys. However, such processes are rare because the D'yakonov-Perel (DP) mechanism cannot result in the spin relaxation of electrons/holes as the out-of-plane spin component is conserved for both carriers [1,26–28]. But in reality, excitons do move between the K to K' valleys and, in certain cases, the depolarization rate is shown to be extremely fast even in exfoliated 1L-MoS₂ samples [29–31]. A recent theory suggests that the long-range part of the electron-hole exchange interaction can virtually transfer excitons between K to K' valleys without directly involving any phonon [32]. In this process, excitons can experience the in-plane effective

magnetic field $\Omega(P_{ex})$ that depends upon its in-plane center-of-mass momentum P_{ex}. Precession of the exciton total angular momentum about $\Omega(P_{ex})$ can cause valley depolarization due to inhomogeneous broadening. The exciton momentum scattering rate can influence its spin scattering rate through the Maialle-Silva-Sham (MSS) mechanism, which has similar characteristics as the DP process for the electrons as well as holes. In the weak scattering regime, the spin scattering rate is proportional to the momentum scattering rate, while the two rates follow the inverse relationship in the strong scattering regime. The presence of defects can thus influence the momentum relaxation rate of the excitons and hence can affect the valley depolarization.

Here we explore the influence of sulfur-vacancy-related defects on the valley polarization property of CVD-grown 1L-MoS$_2$. Our study reveals that momentum scattering of the excitons due to the sulfur vacancies, which are physisorbed with air molecules, influences the intervalley spin-flip transition rate of the excitons and hence the valley depolarization process. Both weak and strong scattering regimes of the intervalley excitonic transfer processes could indeed be identified from the dependence of the degree of valley polarization on the defect concentration as well as on the temperature, validating the MSS mechanism. It has been found that in the presence of biaxial tensile strain, high defect densities and/or at sufficiently high temperatures, (LA) phonon-assisted intervalley scattering via the Γ valley becomes important. This has been corroborated by *ab initio* band-structural calculations.

II. EXPERIMENTAL TECHNIQUES

Three types of samples were used for the study. Monolayer-MoS$_2$ films, which had been grown on c-sapphire substrates using a microcavity-based CVD technique [33], were labeled as sample M1. One of the as-grown 1L-MoS$_2$ samples, which was vacuum annealed at $200\,^\circ$C in a pulsed laser deposition (PLD) chamber for 10 minutes and eventually coated with the deposit resulting from laser ablation of the hBN pellet, was labeled as sample M2. A $\sim$20-nm-thick coating of a material consisting of B, N, and oxygen was found to be deposited on top of the MoS$_2$ film (see the Supplemental Material for more information about the deposited layer and the deposition process [34]; see, also, Refs. [35–42] therein). Another as-grown 1L-MoS$_2$ film was dislodged from the sapphire substrate and placed on a SiO$_2$ coated Si substrate using a surface-energy-assisted transfer method using polystyrene (PS) as the carrier polymer [43]. This sample was termed sample M3. More details about the growth, transfer process, and characterizations of these samples can be found in the Supplemental Material [34].

Photoluminescence (PL) and polarization-resolved PL studies were conducted keeping the samples in a liquid-nitrogen cryostat. Measurements were carried out in a backscattering configuration within a microscope setup equipped with a $50\times$ long working distance objective (NA= 0.5). For PL, a 532 nm diode laser was used as the excitation source. For polarization-resolved PL, an achromatic quarter wave plate was used to produce circularly polarized lights ($\sigma^{-/+}$) from the linearly polarized HeNe (632.8 nm) laser. Another achromatic quarter wave plate in combination
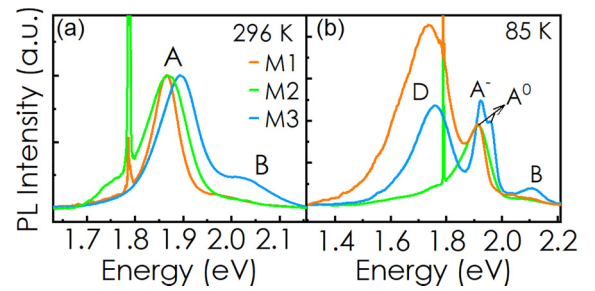

FIG. 1. Normalized (with respect to the A-excitonic feature) photoluminescence spectra recorded with 532 nm laser excitation for different samples at (a) room temperature and (b) 85 K.

with a Glan-Taylor analyzer was placed before the spectrometer entrance slit to select between σ^- and σ^+ emitted photons. The spectra were recorded using a 0.55 m focal length monochromator equipped with a Peltier cooled CCD detector. To avoid Joule heating, the excitation intensity was kept at 150 µW on a spot diameter of $\sim$5 µm.

III. RESULTS AND DISCUSSION

In the room-temperature PL spectra recorded with 532 nm laser excitation for the three samples as shown in Fig. 1(a), A-excitonic features are found at almost the same energy positions for the as-grown and the capped samples, whereas the feature appears at a higher energy position for the transferred sample. This blueshift implies the release of the tensile strain after transfer of the monolayer from the sapphire to the amorphous SiO$_2$/Si substrate [12,13]. Note that the as-grown 1L-MoS$_2$ layer on sapphire is expected to be under tensile biaxial strain due to the mismatch in the thermal expansion coefficient and/or lattice constant [44–46]. The broad luminescence feature (D) appearing at $\sim$1.75 eV in Fig. 1(b), where 85 K PL spectra are compared, can be attributed to those V_S sites where air molecules are physisorbed [10,14,47]. Evidently, the intensity of the D peak is significantly less in the transferred sample M3 as compared to that of the as-grown sample M1. The D peak is almost fully suppressed in the capped sample M2. Annealing followed by capping in the preparation process of samples M2 and M3 are found to be the reason for the reduction of the D feature [14]. It is interesting to note that the trion peak is stronger than the excitonic feature in sample M3, implying a large enhancement of electron concentration, which can be attributed to polystyrene. As an aromatic hydrocarbon, PS has the potential to act as donors [14].

Figure 2 shows the polarization-resolved PL spectra with σ^- excitation recorded at 85 K on the three samples. The degree of valley polarization, which is defined as $P = (I^- - I^+)/(I^- + I^+)$ with $I^{-/+}$ as the intensity of $\sigma^{-/+}$ light, is also plotted as a function of photon energy in the respective panels. Evidently, in all cases, polarization could only be observed at the A-exciton/trion features, while the D band does not show any polarization at all. Note that the D feature is almost completely suppressed in the sample M2 and the sample shows higher P than what is typically obtained in as-grown samples. This finding highlights the role of V_S-Air defects in
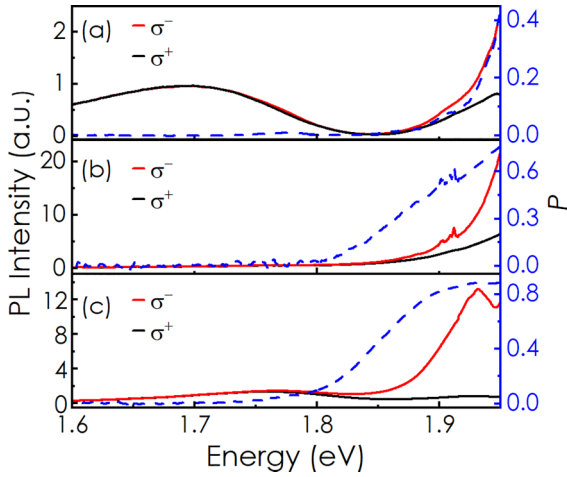
FIG. 2. Circular polarization-resolved PL spectra recorded at 85 K for the samples (a) M1, (b) M2, and (c) M3. The degree of polarization (P) is also plotted as a function of photon energy in these figures (dashed blue lines). The red and black lines represent the spectra obtained for σ^- and σ^+ polarized luminescence, respectively, when σ^- polarized 633 nm laser light is used for excitation.

FIG. 3. (a) Degree of circular polarization (P) as a function of I_D/I_A obtained at various sampling points on different samples. (b) Plot of $\ln(P^{-1} - 1)$ vs $\ln(I_D/I_A)$ for all the sampling points. Temperature dependence of P for (c) as-grown samples with two different I_D/I_A ratios and (d) the transferred sample.

determining the valley polarization property of the material. Interestingly, P goes to as high as 82% in the case of sample M3, where the intensity of the D peak is significantly reduced compared to what is generally found in as-grown samples, but the reduction is not as much as is found in sample M2. The observation of higher P in sample M3 compared to M2, even when the V_S-Air defect density is larger in the former, can be attributed to the relaxation of biaxial strain in the MoS$_2$ film after the transfer [14]. Polarization-resolved PL spectra are recorded at several spots on samples M1, M2, and M3. The relative intensity of the D feature with respect to A-exciton complex I_D/I_A at each sampling point can serve as a measure for the density of V_S-Air defects at that location. Note that in the case of the as-grown sample, even though the ratio is found to vary significantly from spot to spot, the position of the A feature does not change much (see the Supplemental Material, Fig. S5 [34]). In the case of capped and transferred samples, neither the I_D/I_A ratio nor the excitonic peak position show much spatial variation. The degree of polarization P obtained at 85 K from various parts of these samples is plotted versus I_D/I_A in Fig. 3(a) (see the Supplemental Material, Fig. S6, for the polarization-resolved PL spectra recorded at different spots on these samples [34]). In the case of the as-grown and the capped samples (M1 and M2), P is obtained at a fixed energy of 1.945 eV, while for the transferred sample, P measured at the peak of the A-exciton/trion complex is used for the plot. Since the higher-energy side of the PL feature corresponding to the A-exciton/trion complex cannot be visible with the 633 nm (1.96 eV) excitation, the I_D/I_A ratio is obtained from the PL spectra recorded with 532 nm laser excitation at the same spot in all cases. Evidently, for the as-grown and the capped samples, all the data obey a trend of rapid initial decrease followed by a plateauing as the I_D/I_A ratio increases. Interestingly, beyond a certain I_D/I_A ratio, P suddenly drops to zero. Note that the data obtained from the transferred sample stay clearly isolated from other
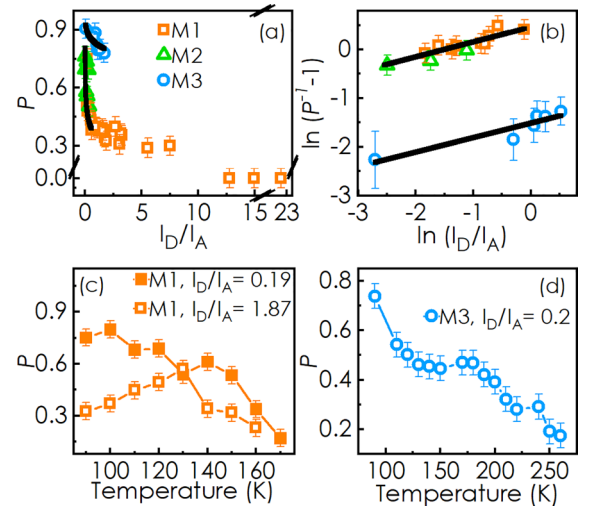
data points in the plot. But, they also show a reduction as I_D/I_A increases. These observations clearly demonstrate the correlation between the V_S-Air defects and P. The data points from the rapid initial decrease part for all the samples are plotted as $\ln(P^{-1} - 1)$ versus $\ln(I_D/I_A)$ in Fig. 3(b). It should be noted that both of the data sets show a straight line. This point will be discussed later.

Figure 3(c) compares the temperature (T) variation of P recorded for an as-grown sample at two spots with different I_D/I_A ratios. Interestingly, P shows a monotonous decrease with the increase in temperature when I_D/I_A is only 0.19, while P initially increases and then decreases with rising temperature for $I_D/I_A = 1.87$. We have investigated several spots with different I_D/I_A ratios, and P is found to consistently exhibit an initial trend of either reduction or enhancement with increasing T depending upon whether I_D/I_A is sufficiently low or high, respectively. Note that a recent study has reported the enhancement of valley polarization via increasing the scattering rate by raising the sample temperature or introducing charge doping in exfoliated 1L-MoS$_2$ [48]. Figure 3(d) plots P as a function of T for the transferred sample M3 at a spot with $I_D/I_A = 0.2$. P, in this case, shows a reduction followed by a plateauing tendency as T increases. Beyond ∼250 K, the polarization suddenly drops to zero.

Upon illumination with a circularly polarized light falling perpendicularly to the layer plane, A-excitons/trions are generated in one of the K valleys depending upon the helicity of the incident light. The generated excitons can either be transferred to other nonequivalent K valleys through intervalley transition processes or can be captured by the V_S-Air defect centers before recombination. One can consider that the excitons are generated at a rate of G in only one of the valleys (say, K valley). At the steady-state condition, the concentration of excitons in the K, K' valleys (X and X') and the defect sites (X_D) can be governed by the following rate

equations:

$$G - \gamma X - \beta(N_o - X_D)X - (X - X')\gamma_s = 0, \quad (1)$$

$$-\gamma X' - \beta(N_o - X_D)X' - (X' - X)\gamma_s = 0, \quad (2)$$

$$\beta(N_o - X_D)(X + X') - \gamma_D X_D = 0, \quad (3)$$

where γ and γ_s are the total recombination (radiative plus nonradiative) and the intervalley relaxation rates of the A-excitons. γ_D is the total recombination rate of the bound excitons, N_o is the defect concentration in the sample, and β is the coefficient of transition of A-excitons to the defect bound state. Considering $X_D/N_o \ll 1$, polarization can be obtained as $P=(I^- - I^+)/(I^- + I^+) = (X - X')/(X + X')=1/[1 + 2\gamma_s/(\gamma + \beta N_o)]$ from Eqs. (1) and (2). One may further contemplate that the rate of recombination of A-excitons, γ, is much more than the rate of capture of those excitons in the defect sites, βN_o. Polarization can then be expressed as $P = 1/[1 + 2\gamma_s/\gamma]$.

According to the theory proposed by Yu and Wu, the intervalley spin scattering rate γ_s of the A-excitons should depend on the momentum scattering rate (r_p) of the excitons through the Maialle-Silva-Sham (MSS) mechanism [32]. It is quite reasonable to believe that the presence of air molecules at the S-vacancy sites introduces certain additional local vibrational modes, which can take part in the momentum scattering of excitons. One may thus consider that $r_p \propto (N_o)^\alpha$, where the power α is a constant. In the weak scattering regime, $\gamma_s \propto r_p$ and hence $\gamma_s = Q_s(N_o)^\alpha$, where Q_s is a constant. One can also express defect concentration N_o in terms of the intensity ratio I_D/I_A as $N_o = (\gamma_r \gamma_D/\beta \gamma_{rD})(I_D/I_A)$, where γ_r and γ_{rD} are the radiative recombination rate of A-excitons/trions and the defect bound excitons, respectively (see the Supplemental Material [34]). P can now be given by

$$P = \frac{1}{[1 + S(I_D/I_A)^\alpha]}, \quad (4)$$

where $S = 2(Q_s/\gamma)(\gamma_r \gamma_D/\beta \gamma_{rD})^\alpha$. Note that γ_r and γ_{rD} are independent of the defect concentration. At low defect densities and sufficiently low temperatures, the recombination of excitons takes place mostly through radiative pathways and hence $\gamma \approx \gamma_r$ and $\gamma_D \approx \gamma_{rD}$. S can thus be treated as independent of N_o. The rapid initial fall in the P versus I_D/I_A plot shown in Fig. 3(a) can now be explained through Eq. (4). Note that the data points from the weak scattering regime in all these samples show a linear behavior when plotted as $\ln(P^{-1} - 1)$ versus $\ln(I_D/I_A)$, as shown in Fig. 3(b). Data obtained for samples M1 and M2 clearly follow a straight line, while those from sample M3 can be fitted with a separate but parallel straight line with a slope of $\alpha = 0.33$. This further establishes the validity of Eq. (4), especially in the weak scattering regime. It should be noted that the MSS mechanism predicts $\gamma_s \propto r_p^{-1}$ in the strong scattering regime, meaning P should increase with r_p, while r_p is expected to increase with T. In Figs. 3(c) and 3(d), the observation of the initial decrease and increase of P with the rising temperature when I_D/I_A is low and high, respectively, can be assigned to the weak and strong scattering regimes, respectively.

At sufficiently high temperatures, P has been found to decrease with increasing T in all cases. This can be attributed

to the increase of the center-of-mass momentum of the excitons p_{ex}. Since the band gap of the material decreases with the increase of T, for the same photon energy of excitation, the probability of generation of excitons with higher p_{ex} increases and, according to the theory [32], γ_s increases with p_{ex}. Further, the polarization data presented in Fig. 3(a) show a plateauing tendency beyond $I_D/I_A \approx 1.5$ before abruptly dropping down to zero at $I_D/I_A \approx 6$. However, theory predicts P to enhance with I_D/I_A beyond a certain point as the defect density moves from the weak to strong scattering regime. This may indicate the presence of other competing mechanisms, which increase the excitonic spin relaxation rate with I_D/I_A. One of the possible candidates might be the exchange interaction of the excitons with the air molecules attached at the V_S sites. Note that certain air molecules, such as O_2 and H_2O, possess magnetic moment [49,50]. Physisorption of such molecules at the V_S sites can interact with the excitons through exchange coupling. The spin relaxation rate of the excitons due to these scattering processes is expected to be proportional to the density of these defects [51,52]. It should be mentioned that the increase of disorder in the lattice as a result of the increase of defect density (I_D/I_A), which leads to the change in the band structure, also results in the reduction of the valley polarization [24]. We believe that the sudden drop of P to zero when plotted as a function of I_D/I_A (at ~6) in Fig. 3(a) is due to the inclusion of a large density of disorder in the lattice at such a high defect concentration. In fact, the reduction of the valley polarization with the increase of disorder in 1L-MoS$_2$ has been reported [31].

We have carried out band-structural calculations under the framework of density functional theory (DFT) [53], considering the spin-orbit coupling effect to understand the role of different perturbations such as V_S formation, physiadsorption of air molecules with the V_S sites, and biaxial strain on the band structure of 1L-MoS$_2$. The van der Waals interaction between the oxygen molecule and MoS$_2$ surface is taken into account by employing Grimme's dispersion corrections of the DFT-D3 type [54]. A 4×4 supercell of MoS$_2$ is considered for the simulations, and a vacuum space of 20 Å is introduced along the z direction to avoid the periodic interactions in our system. A single V_S is introduced in the 4×4 supercell of MoS$_2$, and one oxygen molecule is introduced on top of V_S. Details of the calculation are provided in the Supplemental Material [34] (see, also, Refs. [55–58] therein).

Calculated band structures for 1L-MoS$_2$, when the layer is pristine, biaxially strained (tensile), unstrained but with bare V_S defects, and unstrained but with V_S-O$_2$ defects are compared in Fig. 4. It is noticeable that as compared to the pristine layer, the energy separation between the K/K' and the Γ valley is reduced whenever the layer is either under a tensile biaxial strain or incorporated with the defects. Reduction of the energy gap can enhance the chance of the holes to transfer between the K and K' valleys via the Γ valley through phonon-assisted intervalley processes [24]. However, it has to be noted that the z component of the hole spin is still a good quantum number even for the Γ valley. The DP mechanism cannot thus be a dominant process for spin relaxation in this pathway [32]. Rather, the Elliott-Yafet (EY) mechanism should play a more significant role in the hole spin relaxation process at the Γ valley.
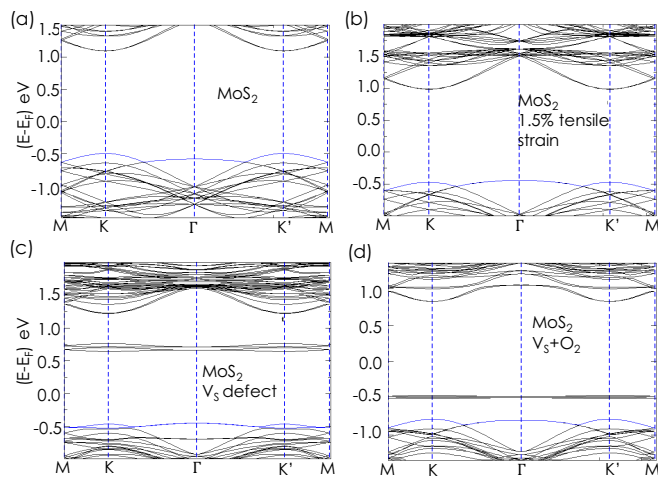
FIG. 4. Calculated band structures of 1L-MoS$_2$: when the film is (a) pristine, (b) biaxially strained (tensile), (c) unstrained but with bare V_S defects, and (d) unstrained but with V_S-O$_2$ defects.

demonstrates that at sufficiently low defect densities and temperatures, the long-range electron-hole exchange mediated transfer of excitons between K/K' valleys indeed happens due to momentum scattering via the MSS mechanism, as theoretically proposed [32]. The momentum scattering rate of the excitons due to these defects comes out to be proportional to the cube root of the defect density. The intervalley transfer process of excitons involving the Γ valley also plays a substantial role, especially when the layer has tensile strain or a high density of V_S defects as K to Γ-energy separation decreases with these perturbations. The study further suggests that the exchange interaction between the excitons and the physisorbed air molecules can also lead to intervalley spin-flip scattering. Such processes also give a substantial contribution to valley depolarization especially at a strong scattering regime.

IV. CONCLUSION

In conclusion, the momentum scattering of excitons due to V_S-air defects has been found to play a vital role in the valley depolarization process of CVD-grown 1L-MoS$_2$. The study

[1] D. Xiao, G.-B. Liu, W. Feng, X. Xu, and W. Yao, Coupled Spin and Valley Physics in Monolayers of MoS$_2$ and other Group-VI Dichalcogenides, Phys. Rev. Lett. **108**, 196802 (2012).

[2] Z. Y. Zhu, Y. C. Cheng, and U. Schwingenschlögl, Giant spin-orbit-induced spin splitting in two-dimensional transition-metal dichalcogenide semiconductors, Phys. Rev. B **84**, 153402 (2011).

[3] K. F. Mak, K. He, J. Shan, and T. F. Heinz, Control of valley polarization in monolayer MoS$_2$ by optical helicity, Nat. Nanotechnol. **7**, 494 (2012).

[4] W. Yao, D. Xiao, and Q. Niu, Valley-dependent optoelectronics from inversion symmetry breaking, Phys. Rev. B **77**, 235406 (2008).

[5] T. Cao, G. Wang, W. Han, H. Ye, C. Zhu, J. Shi, Q. Niu, P. Tan, E. Wang, B. Liu, and J. Feng, Valley-selective circular dichroism of monolayer molybdenum disulphide, Nat. Commun. **3**, 887 (2012).

[6] S. Shree, A. George, T. Lehnert, C. Neumann, M. Benelajla, C. Robert, X. Marie, K. Watanabe, T. Taniguchi, U. Kaiser *et al.*, High optical quality of MoS$_2$ monolayers grown by chemical vapor deposition, 2D Mater. **7**, 015011 (2019).

[7] S. Tongay, J. Zhou, C. Ataca, J. Liu, J. S. Kang, T. S. Matthews, L. You, J. Li, J. C. Grossman, and J. Wu, Broad-range modulation of light emission in two-dimensional semiconductors by molecular physisorption gating, Nano Lett. **13**, 2831 (2013).

[8] P. K. Chow, R. B. Jacobs-Gedrim, J. Gao, T.-M. Lu, B. Yu, H. Terrones, and N. Koratkar, Defect-induced photoluminescence in monolayer semiconducting transition metal dichalcogenides, ACS Nano **9**, 1520 (2015).

[9] H. Nan, Z. Wang, W. Wang, Z. Liang, Y. Lu, Q. Chen, D. He, P. Tan, F. Miao, X. Wang *et al.*, Strong photoluminescence enhancement of MoS$_2$ through defect engineering and oxygen bonding, ACS Nano **8**, 5738 (2014).

[10] S. Deb, P. Chakrabarti, P. K. Mohapatra, B. K. Barick, and S. Dhar, Tailoring of defect luminescence in CVD grown monolayer MoS$_2$ film, Appl. Surf. Sci. **445**, 542 (2018).

[11] B. Miller, E. Parzinger, A. Vernickel, A. W. Holleitner, and U. Wurstbauer, Photogating of mono-and few-layer MoS$_2$, Appl. Phys. Lett. **106**, 122103 (2015).

[12] M. Amani, M. L. Chin, A. L. Mazzoni, R. A. Burke, S. Najmaei, P. M. Ajayan, J. Lou, and M. Dubey, Growth-substrate induced performance degradation in chemically synthesized monolayer MoS$_2$ field effect transistors, Appl. Phys. Lett. **104**, 203506 (2014).

[13] C. R. Zhu, G. Wang, B. L. Liu, X. Marie, X. F. Qiao, X. Zhang, X. X. Wu, H. Fan, P. H. Tan, T. Amand, and B. Urbaszek, Strain tuning of optical emission energy and polarization in monolayer and bilayer MoS$_2$, Phys. Rev. B **88**, 121301(R) (2013).

[14] P. Chakrabarti, F. Mujeeb, and S. Dhar, Enhancement of valley polarization in CVD grown monolayer MoS$_2$ films, Appl. Phys. Lett. **121**, 072103 (2022).

[15] D. H. Kim and D. Lim, Effects of defects and impurities on the optical properties and the valley polarization in monolayer MoS$_2$, J. Korean Phys. Soc. **66**, 1564 (2015).

[16] J. Klein, A. Kuc, A. Nolinder, M. Altzschner, J. Wierzbowski, F. Sigger, F. Kreupl, J. J. Finley, U. Wurstbauer, A. W. Holleitner *et al.*, Robust valley polarization of helium ion modified atomically thin MoS$_2$, 2D Mater. **5**, 011007 (2017).

[17] R. Mupparapu, M. Steinert, A. George, Z. Tang, A. Turchanin, T. Pertsch, and I. Staude, Facile resist-free nanopatterning of monolayers of MoS_2 by focused ion-beam milling, Adv. Mater. Interf. **7**, 2000858 (2020).

[18] N. Saigal, I. Wielert, D. Čapeta, N. Vujičić, B. V. Senkovskiy, M. Hell, M. Kralj, and A. Grüneis, Effect of lithium doping on the optical properties of monolayer MoS_2, Appl. Phys. Lett. **112**, 121902 (2018).

[19] H. Shi, H. Pan, Y.-W. Zhang, and B. I. Yakobson, Quasiparticle band structures and optical properties of strained monolayer MoS_2 and WS_2, Phys. Rev. B **87**, 155304 (2013).

[20] E. Scalise, M. Houssa, G. Pourtois, V. Afanas, A. Stesmans *et al.*, First-principles study of strained 2D MoS_2, Phys. E **56**, 416 (2014).

[21] M. M. Glazov, T. Amand, X. Marie, D. Lagarde, L. Bouet, and B. Urbaszek, Exciton fine structure and spin decoherence in monolayers of transition metal dichalcogenides, Phys. Rev. B **89**, 201302(R) (2014).

[22] H.-Z. Lu, W. Yao, D. Xiao, and S.-Q. Shen, Intervalley Scattering and Localization Behaviors of Spin-Valley Coupled Dirac Fermions, Phys. Rev. Lett. **110**, 016806 (2013).

[23] H. Yu, G.-B. Liu, P. Gong, X. Xu, and W. Yao, Dirac cones and Dirac saddle points of bright excitons in monolayer transition metal dichalcogenides, Nat. Commun. **5**, 3876 (2014).

[24] S. Xu, C. Si, Y. Li, B.-L. Gu, and W. Duan, Valley depolarization dynamics in monolayer transition-metal dichalcogenides: Role of the satellite valley, Nano Lett. **21**, 1785 (2021).

[25] Z. Lin, Y. Liu, Z. Wang, S. Xu, S. Chen, W. Duan, and B. Monserrat, Phonon-Limited Valley Polarization in Transition-Metal Dichalcogenides, Phys. Rev. Lett. **129**, 027401 (2022).

[26] L. Wang and M. Wu, Intrinsic electron spin relaxation due to the D'yakonov–Perel' mechanism in monolayer MoS_2, Phys. Lett. A **378**, 1336 (2014).

[27] A. Kormányos, V. Zólyomi, N. D. Drummond, P. Rakyta, G. Burkard, and V. I. Falko, Monolayer MoS_2: Trigonal warping, the γ valley, and spin-orbit coupling effects, Phys. Rev. B **88**, 045416 (2013).

[28] H. Ochoa and R. Roldán, Spin-orbit-mediated spin relaxation in monolayer MoS_2, Phys. Rev. B **87**, 245421 (2013).

[29] D. Lagarde, L. Bouet, X. Marie, C. R. Zhu, B. L. Liu, T. Amand, P. H. Tan, and B. Urbaszek, Carrier and Polarization Dynamics in Monolayer MoS_2, Phys. Rev. Lett. **112**, 047401 (2014).

[30] C. Mai, A. Barrette, Y. Yu, Y. G. Semenov, K. W. Kim, L. Cao, and K. Gundogdu, Many-body effects in valleytronics: Direct measurement of valley lifetimes in single-layer MoS_2, Nano Lett. **14**, 202 (2014).

[31] Q. Wang, S. Ge, X. Li, J. Qiu, Y. Ji, J. Feng, and D. Sun, Valley carrier dynamics in monolayer molybdenum disulfide from helicity-resolved ultrafast pump–probe spectroscopy, ACS Nano **7**, 11087 (2013).

[32] T. Yu and M. W. Wu, Valley depolarization due to intervalley and intravalley electron-hole exchange interactions in monolayer MoS_2, Phys. Rev. B **89**, 205303 (2014).

[33] P. K. Mohapatra, S. Deb, B. P. Singh, P. Vasa, and S. Dhar, Strictly monolayer large continuous MoS_2 films on diverse substrates and their luminescence properties, Appl. Phys. Lett. **108**, 042101 (2016).

[34] See Supplemental Material at http://link.aps.org/supplemental/10.1103/PhysRevB.107.115429 for the details of the transfer technique and more information on the Raman and PL studies of the 1L-MoS_2 samples, as well as for the growth, transfer, capping processes, Raman spectra, PL spectra, polarization-resolved PL spectra, solution of the rate equations, and the density functional theory (DFT) calculation.

[35] M. Belyansky, M. Trenary, and C. Ellison, Boron chemical shifts in b6o, Surf. Sci. Spectra **3**, 147 (1994).

[36] V. Linss, S. Rodil, P. Reinke, M. Garnier, P. Oelhafen, U. Kreissig, and F. Richter, Bonding characteristics of dc magnetron sputtered b–c–n thin films investigated by Fourier-transformed infrared spectroscopy and x-ray photoelectron spectroscopy, Thin Solid Films **467**, 76 (2004).

[37] A. Perrone, A. Caricato, A. Luches, M. Dinescu, C. Ghica, V. Sandu, and A. Andrei, Boron carbonitride films deposited by pulsed laser ablation, Appl. Surf. Sci. **133**, 239 (1998).

[38] M. N. Uddin, I. Shimoyama, Y. Baba, T. Sekiguchi, and M. Nagano, X-ray photoelectron spectroscopic observation on b–c–n hybrids synthesized by ion beam deposition of borazine, J. Vac. Sci. Technol. **23**, 497 (2005).

[39] W. A. Brainard and D. R. Wheeler, An XPS study of the adherence of refractory carbide silicide and boride RF-sputtered wear-resistant coatings, J. Vac. Sci. Technol. **15**, 1800 (1978).

[40] X. Gouin, P. Grange, L. Bois, P. L'Haridon, and Y. Laurent, Characterization of the nitridation process of boric acid, J. Alloys Compd. **224**, 22 (1995).

[41] P. Petrov, D. Dimitrov, D. Papadimitriou, G. Beshkov, V. Krastev, and C. Georgiev, Raman and x-ray photoelectron spectroscopy study of carbon nitride thin films, Appl. Surf. Sci. **151**, 233 (1999).

[42] V. O. Todi, B. P. Shantheyanda, and K. B. Sundaram, Influence of annealing on the optical properties of reactively sputtered BCN thin films, Mater. Chem. Phys. **141**, 596 (2013).

[43] A. Gurarslan, Y. Yu, L. Su, Y. Yu, F. Suarez, S. Yao, Y. Zhu, M. Ozturk, Y. Zhang, and L. Cao, Surface-energy-assisted perfect transfer of centimeter-scale monolayer and few-layer MoS_2 films onto arbitrary substrates, ACS Nano **8**, 11522 (2014).

[44] J. E. Ayers, T. Kujofsa, P. Rago, and J. Raphael, *Heteroepitaxy of Semiconductors: Theory, Growth, and Characterization* (CRC Press, Boca Raton, FL, 2016).

[45] D. Dumcenco, D. Ovchinnikov, K. Marinov, P. Lazic, M. Gibertini, N. Marzari, O. L. Sanchez, Y.-C. Kung, D. Krasnozhon, M.-W. Chen *et al.*, Large-area epitaxial monolayer MoS_2, ACS Nano **9**, 4611 (2015).

[46] H. Ye and J. Yu, Germanium epitaxy on silicon, Sci. Technol. Adv. Mater. **15**, 024601 (2014).

[47] S. Tongay, J. Suh, C. Ataca, W. Fan, A. Luce, J. S. Kang, J. Liu, C. Ko, R. Raghunathanan, J. Zhou *et al.*, Defects activated photoluminescence in two-dimensional semiconductors: Interplay between bound, charged and free excitons, Sci. Rep. **3**, 2657 (2013).

[48] Y.-C. Wu, T. Taniguchi, K. Watanabe, and J. Yan, Enhancement of exciton valley polarization in monolayer MoS_2 induced by scattering, Phys. Rev. B **104**, L121408 (2021).

[49] K. Pitzer, The nature of the chemical bond and the structure of molecules and crystals: An introduction to modern structural chemistry, J. Am. Chem. Soc. **82**, 4121 (1960).

[50] H. Chai, W. Chen, Y. Li, Y. Tang, and X. Dai, The adsorption properties and stable configurations of hydroxyl groups at Mo edge of MoS_2 (100) surface, Mater. Chem. Phys. **283**, 126051 (2022).

[51] M. Wu, J. Jiang, and M. Weng, Spin dynamics in semiconductors, Phys. Rep. **493**, 61 (2010).

[52] W. Koschel and M. Bettini, Zone-centered phonons in $A^I B^{III} S_2$ chalcopyrites, Phys. Stat. Sol. (B) **72**, 729 (1975).

[53] W. Kohn and L. J. Sham, Self-consistent equations including exchange and correlation effects, Phys. Rev. **140**, A1133 (1965).

[54] S. Grimme, J. Antony, S. Ehrlich, and H. Krieg, A consistent and accurate *ab initio* parametrization of density functional dispersion correction (DFT-D) for the 94 elements h-pu, J. Chem. Phys. **132**, 154104 (2010).

[55] G. Kresse and J. Furthmüller, Efficient iterative schemes for *ab initio* total-energy calculations using a plane-wave basis set, Phys. Rev. B **54**, 11169 (1996).

[56] G. Kresse and J. Furthmüller, Efficiency of *ab initio* total energy calculations for metals and semiconductors using a plane-wave basis set, Comput. Mater. Sci. **6**, 15 (1996).

[57] P. E. Blöchl, Projector augmented-wave method, Phys. Rev. B **50**, 17953 (1994).

[58] J. P. Perdew, K. Burke, and M. Ernzerhof, Generalized Gradient Approximation Made Simple, Phys. Rev. Lett. **77**, 3865 (1996).